



Research Article

<https://doi.org/10.1631/jzus.A2500282>

Simulation and experimental analysis of grease injection process in the main drive seal lubrication structure of tunnel boring machines

Zheming TONG^{1,2}, Yuchen ZHAO^{1,2}, Lianhui JIA³, Xiaolei Zhou³, Haoxiang Lu^{1,2}, Wenqi NIU³

¹State Key Laboratory of Fluid Power and Mechatronic Systems, Zhejiang University, Hangzhou 310027, China

²School of Mechanical Engineering, Zhejiang University, Hangzhou 310027, China

³China Railway Engineering Equipment Group Co Ltd, Zhengzhou 450016, China

Abstract: During the excavation process of tunnel boring machines (TBMs), the precision of manufacture and accuracy of assembly components comprising the main drive seal lubrication structure, and operational conditions, directly impact the overall sealing performance. This, in turn, affects the lifespan of the main bearings and the entire TBM. Simulating the process of injecting grease into the internal structure of the main drive seal lubrication chamber under different working conditions is crucial. Analyzing the distribution of grease within the chamber and the pressure distribution within the system enhances the ability of the main drive seal structure to prevent external contaminants from infiltrating, ultimately extending the lifespan of the main drive structure. This study integrated VOF multiphase flow simulations and experimental investigations to systematically analyze the effects of different eccentricities, the number of grease injection ports, and inner wall rotation speed on EP2 grease distribution. When the eccentricity between the inner and outer seal axes was within 0.75 mm, the number of external grease injection ports was increased and the inner wall rotation speed decreased, the grease was evenly distributed in the flow channels. An injection optimization strategy based on pressure monitoring was proposed. In the design of the main drive sealing structure, controlling the eccentricity below 0.75 mm, arranging 12 injection ports along a single chamber while setting the inner wall rotation speed as 5 r/min can effectively improve the sealing performance of the main drive system.

Key words: Tunnel boring machine (TBM), Main drive seal lubrication structure, EP2 injection, Experimental analysis on grease optimization

1 Introduction

With the continuous development of railway and subway construction throughout China, the expansion and improvement of the national railway network have led to an increasing demand for large excavation equipment, particularly tunnel boring machines (TBMs) (Li, 2021; Gong et al., 2024; Zhang et al., 2024; Zhao et al., 2026). The key component of TBM is its main drive system (Fig. 1), which provides significant operational torque to the front cutter head. The main drive system (Jiang, 2015) bears most of the earth pressure generated during the tunneling process

(Nilot et al., 2024) to ensure the entire machine can advance normally.

The performance of this system, often referred to as the "heart" of the TBM, directly impacts the machine's lifespan (Liu et al., 2022; Ai, 2023). If severe wear occurs in this system during operation, it is difficult to perform quick inspections, and can lead to serious construction delays and substantial economic losses. During operation, the TBM operates in a relatively harsh underground environment (Barzegari et al., 2021; Agrawal et al., 2022; Zhou et al., 2025). Due to several design flaws, the traditional main drive sealing structure is prone to failure, which in turn compromises the stable operation of the main drive system (Ma, 2018). Common failure modes include seal ring fracture, excessive wear of the lip, wear of the sealing bushing, and flipping of the sealing lip (Stakenborg et al., 1990; Van and Stakenborg, 1990; Vishwakarma et al., 2017; Zhang, 2018; Yao, 2021; Wang, 2021). To prevent failure of

✉ Yuchen ZHAO, 12025060@zju.edu.cn

Lianhui JIA, jialianhui@crectbm.com

📧 Zheming TONG, <https://orcid.org/0000-0003-1129-7439>

Received June 30, 2025; Revision accepted Nov. 4, 2025;
Crosschecked

the main drive system and ensure its proper operation while minimizing heat generation during tunneling, researchers have studied the sealing and lubrication devices installed at the front end of the main drive to enhance sealing performance and tunneling efficiency.

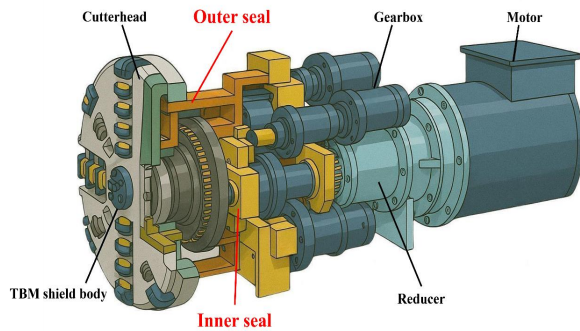


Fig. 1 Main drive system of tunnel boring machine

The sealing performance of the shield machine's main drive can be studied based on practical engineering applications. The structure of sealing rings is discussed first. Currently, single-lip seals and multi-lip (finger-type) seals are widely adopted (Yuan, 2019). Multi-lip seals offer a more intuitive indication of assembly status and provide stable and reliable operation. However, due to their large contact area with the rotating raceway, they generate significant heat during operation, requiring an additional cooling water chamber for timely cooling (Li et al., 2022). In contrast, single-lip seals do not need a separate cooling device and have a more compact overall structure. In this study, we focused on the analysis of the single-lip sealing structure (Tasora et al., 2013). The configuration of this type of sealing and lubrication system is shown in Fig. 2 (Guo et al., 2016). The various lip seals within the main drive sealing and lubrication structure can form multiple sealing chambers with different functions. The sealing structure consists of three lip seals and several spacer rings. The first and second-stage lip seals are oriented towards the tunneling side of the main drive to prevent external impurities from entering and damaging the main bearing area. The third-stage lip seal, located at the far right, faces the internal gear oil tank, preventing leakage from the tank (Liu et al., 2013). The material characteristic of the main drive seal ring is also a key focus of research. Li et al. (2024) analyzed the wear failure characteristics of polyurethane elastomers (Naheed et al., 2021) under

different dry friction conditions, using this as a basis for monitoring temperature-induced failure of the main drive seal. Through analysis of the chain extension coefficient of polyurethane materials (Ariati et al., 2021) used in the main drive seal of the tunneling machine, Wu and Zhang (2022) selected a polyurethane elastomer sealing material with excellent heat and aging resistance. Wang et al. (2023) conducted research on the cooling system, investigating the heat generation and water-cooling efficiency of a polyurethane sealing system under high linear velocity conditions in shield machines. They aimed to optimize the seal system structure to meet the application requirements of polyurethane in the tunneling process. To address the issue of seal failure caused by wear between the seal lip and the rotating raceway, Zeng (2021) used the high hardness and excellent wear resistance of SK5 steel to replace the traditional quenched steel wear strip with an SK5 wear-resistant strip. By welding it onto the support ring, they effectively reduced the manufacturing cost while ensuring the overall reliability of the sealing structure. In addition, to improve the overall performance of the main drive sealing system and extend its service life, various enhancement measures have been adopted. Zhang et al. (2022) used TRIZ theory to analyze the shortcomings of the traditional assembly methods used for components within the main drive sealing structure. After comparing multiple assembly schemes, they designed a type of seal ring installation device that not only ensures sufficient fit of the lip seal but also effectively improves assembly efficiency. Liu et al. (2022) designed a fully pneumatic control device capable of providing timely pressure compensation during grease injection, thereby enhancing the pressure-bearing capacity of the entire shield machine. Other measures, such as using wear-resistant sealing materials, fastening adjacent lip seals with annular pressure plates (Li et al., 2014), and installing spacer rings with support structures behind the lip seals (Gao et al., 2008), can also effectively improve sealing performance and extend the service life of the shield machine.

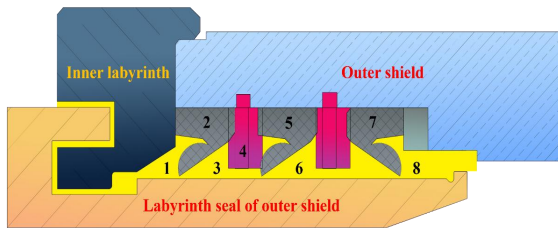


Fig. 2 Single-lip seal internal sealing and lubrication structure: 1- labyrinth chamber 2- first-stage seal 3- sealing and lubrication chamber 4- seal retaining ring 5- second-stage seal 6- sealing detection chamber 7- third-stage seal 8- gear oil chamber

To gain deeper insights into the effects of the structural parameters of the shield machine's main drive seal, scholars have begun studying the whole process through numerical simulation and experiment, aiming to better understand the internal mechanisms (Tong et al., 2023). Borrás et al. (2020) considered that the contact region of the lip seal operated under full-film lubrication and proposed an elastic-hydrodynamic model. However, the model lacks microscopic analysis of contact. Zhang et al. (2021) conducted finite element analysis on lip seals and found that, compared to unsupported seal structures, lip seals with support structures have smaller contact areas and exhibit greater stability under high-pressure conditions. This design alleviates overheating caused by wear and can effectively prevent leakage incidents. Through numerical simulation, Pinedo et al. (2017) found that eccentricity led to an increase in friction, resulting in severe seal wear. To address the significant deformation of lip seals during pressurization, Xiang et al. (2023) developed a bidirectional fluid-structure interaction computational method. This approach enables the simulation of dimensional deformation of lip seals and the transfer of pressure data at various points, allowing for the estimation of grease leakage under simulated conditions. Using bench tests, Hand et al. (2022) found that the seal exhibited more severe friction and a wider wear profile at the lip region under eccentric conditions. Tan et al. (2022) designed an orthogonal experimental scheme and used finite element analysis to simulate the opening pressure differential and contact width of lip seals with different structural parameters, aiming to obtain an optimized structure that meets operational requirements. Zhang et al. (2023) studied the sealing

performance of lip seals under various compression levels and different oil pressures applied to the front and back sides. They found that as the compression of the seal ring increases within a certain range, the maximum von Mises stress on the contact surface between the lip seal and the inner wall also increases accordingly. However, the maximum contact stress at that location tends to decrease overall. Ji et al. (2023) focused on the contact area between the sealing ring and the rotating inner cylinder, using the Hertz contact model to calculate the contact pressure of the surface asperities at that location. They also conducted fluid-structure-thermal coupling studies to investigate the local heating characteristics of the sealing ring during operation. Some researchers have conducted experimental analyses on other flow field parameters of the main drive sealing system in addition to the simulation optimization of structural parameters related to lip seals. Xu et al. (2021) built a test platform with adjustable labyrinth channel gaps and lengths, and used a controlled variable method to investigate how different parameters of the labyrinth channel structure affect grease diffusion. The experimental results showed that a longer labyrinth and smaller gaps in the labyrinth chamber can effectively expand the range of grease diffusion and promote the formation of a grease ring. In response to issues observed on construction sites, such as excessive levels of Pb, Cr, and moisture in gear oil, Wang et al. (2021) dismantled and modified the original labyrinth structure of the TBM main drive seal. This structural modification took only 24 h and met the operational requirements, significantly reducing the construction time of the project.

Many structural designs for the main drive seal lubrication system have been proposed. However, most of these improvements focused on individual components within the main drive seal structure. As a result, there is an absence of comprehensive analysis of the sealing and lubrication performance of the entire system under various complex working conditions. In this study, we integrated the VOF model for numerical simulation to analyze the grease flow process and compared the results with laboratory experiments, thereby fully validating the effects of sealing parameters under dynamic operating conditions. Our model provides guidance for the optimization of the TBM main drive sealing system

and overcomes the limitations of traditional models that focus on individual parameters. Simulating the process of grease injection into the main drive sealing and lubrication structure under different conditions and analyzing the distribution of grease within the cavity, as well as the internal pressure distribution, is crucial to enhancing the structure's ability to prevent the intrusion of external impurities and prolonging its operational life. We aimed to address these aspects through dynamic simulations and optimization techniques.

This study focused on the influence of parameter selection during grease injection in the main drive lubrication system of the TBM and its impact on lubrication performance. In Section 2, we described the conceptual VOF simulation model and present the properties of the EP2 grease used in this work. Section 3 detailed the procedures and results of the lubrication experiments conducted. Section 4 was dedicated to the simulation analysis: the simulation model was established and, then the simulation results were compared with those from laboratory experiments to confirm their reliability. Subsequently, we analyzed the evolution of the grease volume fraction over different simulation times. Pressure measurement points were selected on the annular cavity to compare the effects of eccentricity, the number of injection ports and inner wall rotation speeds on both the pressure distribution and grease filling rate. Finally, Section 5 summarized the conclusions drawn from this work.

2 Methodology

2.1 Computational Model Selection

For the case of grease injection into the main drive sealing and lubrication structure, the injected grease is almost immiscible with air, resulting in a distinct phase interface between the grease and air phases. Compared with other interface-capturing approaches such as the level-set method, the VOF (volume of fluid) model (Giorgio et al., 2024; Zhang et al., 2019; Song et al., 2011; Zhu et al., 2022) has distinct advantages in ensuring mass conservation and handling complex topological changes, including interface rupture, coalescence, and cavity entrapment. These features (Dai et al., 2025; Tang et al., 2024) are

critical for grease lubrication problems, where the conservation of the injected lubricant volume and the accurate prediction of its spatial distribution are most important. Although the level-set method offers smoother interface representation, it suffers from non-conservation of mass, which may lead to spurious loss of lubricant in long-term simulations. Therefore, VOF was adopted in this work to achieve reliable predictions of grease distribution under different operating conditions. The VOF model is an interface-tracking method commonly used for computations involving immiscible fluids. It can be used to determine the steady-state or transient liquid-gas interface within the computational domain. The flow chart of the whole process is shown in Fig. S1 of the electronic supplementary materials (ESM).

The gas-liquid interface is determined by introducing a volume fraction function α within each computational cell (Wang and Zhong, 2021). Let $\alpha_q \in [0,1]$ denote the volume fraction of the primary phase in a computational cell. The transport of α is governed by the following advection equation, where $\boldsymbol{\mu}$ is the velocity vector field and $\boldsymbol{\mu}_\tau$ is an artificial compression velocity introduced to sharpen the interface.

$$\frac{\partial \alpha}{\partial t} + \nabla \cdot (\alpha \boldsymbol{\mu}) + \nabla \cdot (\alpha(1-\alpha)\boldsymbol{\mu}_\tau) \quad (1)$$

In the absence of the compression term, the equation reduces to a standard advection equation:

$$\frac{\partial \alpha}{\partial t} + \boldsymbol{\mu} \cdot \nabla \alpha = 0 \quad (2)$$

For incompressible flow, the continuity equation takes the following form:

$$\nabla \cdot \boldsymbol{\mu} = 0 \quad (3)$$

The parameters of the mixed fluid within a computational cell are calculated using Eq. (4) and Eq. (5), where ρ_g , ρ_l and ρ_m are densities of gas, liquid and the mixed fluid, respectively. μ_g , μ_l and μ_m represent the viscosities of gas, liquid and the mixed fluid, respectively. α is the volume fraction function above.

$$\rho_m = \alpha \rho_l + (1-\alpha)\rho_g \quad (4)$$

$$\mu_m = \alpha \mu_l + (1-\alpha)\mu_g \quad (5)$$

The momentum equation for the mixture is

written as Eq. (6), where F_{st} is the surface tension force while g is the gravitational acceleration vector. T is the fluid temperature while p is the fluid pressure.

$$\rho_m \left(\frac{\partial \mu}{\partial t} + \mu \cdot \nabla \mu \right) = -\nabla p + \nabla \cdot [\mu_m (\nabla \mu + (\nabla \bar{\mu})^T)] + F_{st} + \rho_m g \quad (6)$$

2.2 Characteristic of the main drive seal grease

The grease used in this study is EP2 which was an extreme pressure lubricant that has advantages such as the ability to block external dust and strong adhesion (Wang et al., 2020). EP2 grease parameters obtained through experimentation are shown in Table S1 of the ESM. Its detailed feature description is provided in Section S1 of the ESM.

3 Indoor experiments

3.1 Experiment condition

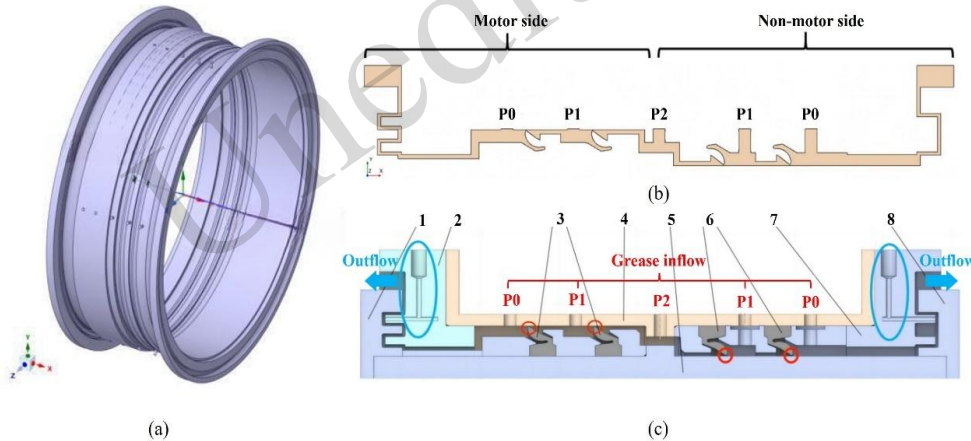


Fig. 3 Numerical model (a) original fluid passage structure (b) upper cross-sectional chamber distribution of the lip seal (c) internal structure:1-sealing motor-side end cover 2-outer cylinder labyrinth 3-main drive seal (reverse lip) 4-outer cylinder 5-inner cylinder 6-main drive seal (forward lip) 7-outer cylinder labyrinth (non-motor side seal) 8-sealing non-motor-side end cover

4.2 Flow field mesh division

Hybrid mesh (Zhu et al., 2017) combines the advantages of both structured and unstructured meshes. The grid structure of the original flow field is shown in Table S3 of the ESM. The generated mesh was verified for independence (Fig. S5 of the ESM). From the line chart, when the number of meshes in the model reaches $5.0E+06$, the grease pressure value in the lubrication chamber gradually stabilizes. Therefore, in this study, a mesh configuration with $5.0E+06$ elements were chosen to discretize the flow

The experiment's test bed is shown in Fig. S2, the statistical dimensions of the experimental design are summarized in Table S2, and the experimental procedure is detailed in Section S2 of the ESM.

3.2 Experimental results

The diffusion trajectories of EP2 grease are illustrated in Fig. S3, experiment result analysis is detailed in Section S3, and the leakage of EP2 grease on the non-motor side is shown in Fig. S4 of the ESM.

4 Simulation analysis

4.1 Simulation model establishment

To better understand the internal mechanism of the main drive seal condition, a numerical model was established (Fig. 3) to observe the passage of the lip seal with various parameters, as described in detail in Section S4 of the ESM.

channel model.

4.3 Results and discussion

4.3.1 Grease injection process under the original operating condition

The boundary conditions for EP2 grease under the original working conditions are shown in Table 1. During the grease injection process into the main drive sealing chamber, as the amount of injected grease increases, the distribution of grease within the chamber generally exhibits a certain regularity. Six time points were selected for analysis using

corresponding grease volume fraction contour plots and the average grease volume fraction line chart (Fig. 4). The detailed analysis of the time-dependent distribution of the lubricant is shown in Section S5 of the ESM. The volume-averaged grease distribution during the 0–9000s injection process is shown in Fig. S6 of the ESM.

Table 1 Boundary conditions under the original working conditions

Number of injection ports	Injection ports per chamber	Single-pipe flow rate	Inner wall rotational speed
40	8	0.64mm/s	5r/min

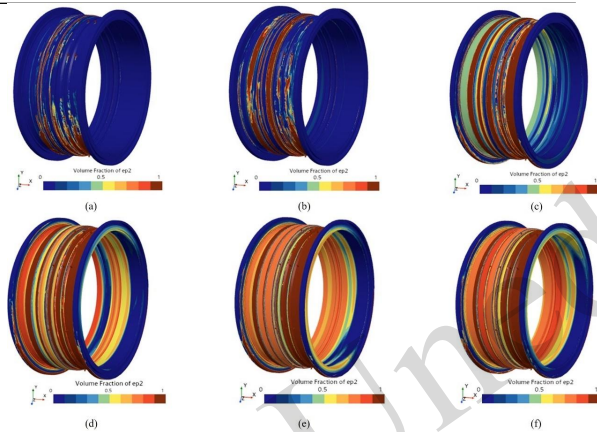


Fig. 4 Grease volume distribution at different time points during the injection process (a) $t=1400s$ (b) $t=2800s$ (c) $t=4200s$ (d) $t=5600s$ (e) $t=7000s$ (f) $t=9000s$

4.3.2 Simulation model verification

To verify the feasibility of the simulation model established in Section 4.1, the experimental measurements of pressure distribution under the original operating condition were compared with the numerical simulation results. A total of eight pressure monitoring points was selected on both the motor side and non-motor side, corresponding one-to-one with the actual pressure sensor locations on the test bench in Fig. 5. Monitoring points 1, 2, 3, and 4 were located near the outlet on the motor side, while points 5, 6, 7, and 8 were positioned near the outlet on non-motor side. The monitoring points on each side are arranged circumferentially at 90° intervals. The data obtained from experiments and numerical simulations at pressure monitoring points

after EP2 grease injection process under different eccentricity conditions were compared (Fig. S7 of the ESM). The numerical simulation results closely agree with the experimental data, thereby confirming the feasibility and validity of the simulation model.

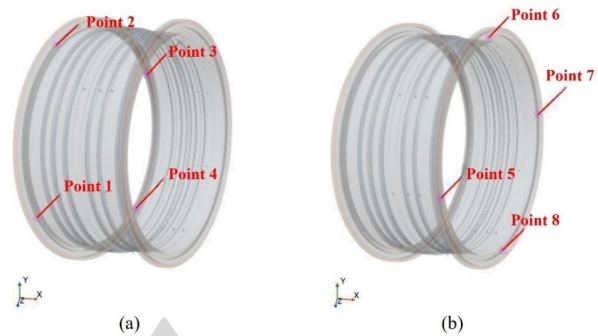


Fig. 5 Distribution of pressure points within the fluid domain (a) motor side (b) sealing non-motor

4.3.3 Influence of concentricity error

The testbed was modified by rotating the inner cylinder along the positive Y-axis direction with displacements of 0.75, 1.5, 2.5, and 3.5 mm, generating corresponding eccentricities between the stationary outer cylinder and the rotating inner cylinder. The EP2 distribution on the YOZ cross-sections is presented in Table S4 of the ESM. Under the original working condition, the motor side had a relatively narrow radial structure, allowing for a higher grease fill rate on that side. In contrast, the non-motor side chamber had a larger radial gap, resulting in areas where grease did not adhere to the rotating wall surface, leading to a lower grease volume fraction. When the eccentricity between the axes of the inner and outer cylinders increased to 1.5 mm, the grease volume fraction in both the motor side and non-motor side chambers decreases. In particular, regions within the motor-side P0 and P2 chambers of the flow field showed no grease adhering to the inner wall, forming partial cavity areas. When the eccentricity exceeded 2.5 mm, comparison of grease distribution in the P0 chambers on both sides revealed a significant imbalance, with severe grease distribution asymmetry. Due to the eccentricity, grease tended to accumulate in the lower part of the fluid domain.

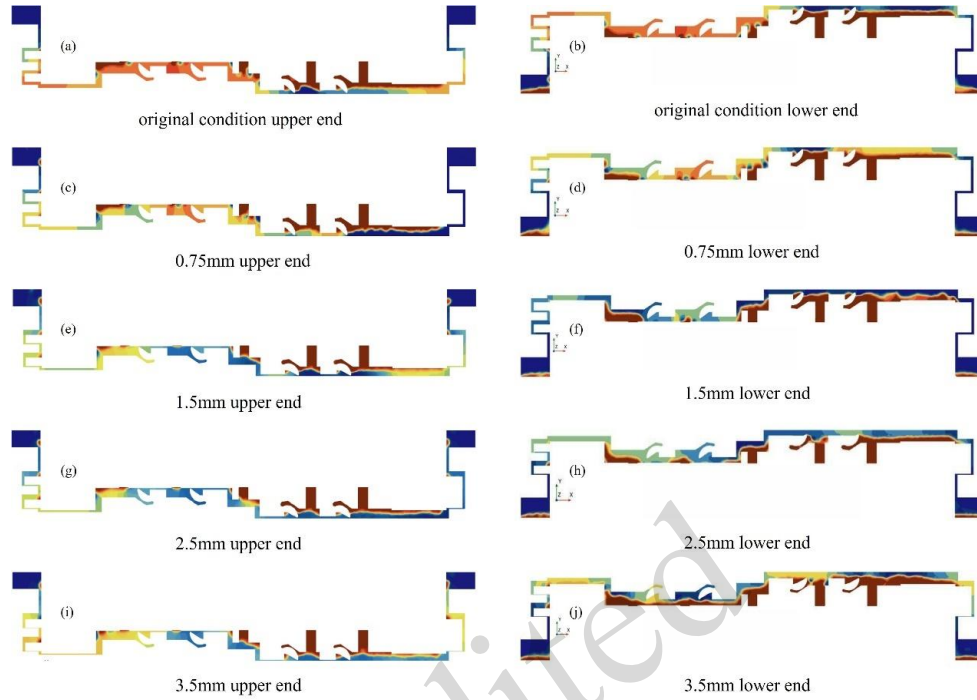


Fig. 6 EP2 grease distribution under different eccentricities of fluid domain (a) original condition upper end (b) original condition lower end (c) $e=0.75\text{mm}$ upper end (d) $e=0.75\text{mm}$ lower end (e) $e=1.5\text{mm}$ upper end (f) $e=1.5\text{mm}$ lower end (g) $e=2.5\text{mm}$ upper end (h) $e=2.5\text{mm}$ lower end (i) $e=3.5\text{mm}$ upper end (j) $e=3.5\text{mm}$ lower end

In the labyrinth chamber, the amount of grease in the lower half was consistently greater than that in the upper half (Fig. 6). Most of the grease on the lower side of the flow path adhered to the stationary outer wall under the combined effects of gravity and inner wall agitation. These observations indicate that, compared to the original condition, increasing the eccentricity between the inner and outer cylinders leads to a general decrease in grease distribution throughout the chamber. Therefore, to ensure uniform grease distribution within the chamber, large eccentricities between the inner and outer cylinders should be avoided.

To quantify the uniformity of EP2 grease distribution, the volume fraction values under different eccentricity conditions were collected. The data in Table 2 were processed according to Eq. (7), yielding a standard deviation $\sigma_{\text{global}}(e)$ of 0.70205% and a mean value μ of 53.476%. When the concentricity error α was 0.75 mm, the corresponding volume fraction fell between the values $\mu + \sigma_{\text{global}}(e)$ and $\mu + 2 * \sigma_{\text{global}}(e)$, thereby confirming its validity as threshold.

$$\begin{cases} \mu = \frac{\sum_{i=1}^N \mu_i}{N} \\ \sigma_{\text{global}}(e) = \sqrt{\frac{1}{N} \sum_{i=1}^N (\mu_i - \mu)^2} \end{cases} \quad (7)$$

Table 2 Uniformity of EP2 grease distribution

Concentricity error/mm	Volume fraction of EP2
	grease (%)
0	54.27
0.75	54.21
1.5	53.09
2.5	52.93
3.5	52.88

A comprehensive analysis of the pressure variation at each point under different conditions revealed that significant fluctuations began to occur around 2500 s (Fig. 7). Therefore, pressure variation curves after 2500 s were extracted for detailed analysis.

Due to the stirring effect of the forward-rotating inner cylinder and the tendency of grease to

accumulate in the lower part of the flow field, the pressure at points 1, 2, and 5 showed various degrees of decrease during injection, whereas the pressure at points 3, 4, 7, and 8 increased significantly. Additionally, analyzing each monitoring point individually revealed that the amplitude of pressure fluctuations increased with greater eccentricity. When the eccentricity was less than 0.75 mm, the grease distribution inside the flow channel remained relatively uniform, maintaining a certain degree of sealing performance. However, when eccentricity exceeded 1.5 mm, an uneven grease distribution was observed between the motor side and the non-motor side. As the eccentricity increased, grease tended to accumulate more prominently at the lower end of the

lubrication chamber. Under such conditions, the main drive sealing structure may fail to ensure proper sealing and lubrication.

The presence of eccentricity between the inner and outer cylinders had a significant impact on grease pressure near the outlet area, with greater eccentricity leading to larger fluctuations in pressure. Due to structural differences caused by the variable radial width of the flow paths on the motor side and the non-motor side, the corresponding pressure values at the same positions on both sides differed considerably, although the overall trends remained consistent. An increase in eccentricity further amplified the range of pressure variation between the two sides.

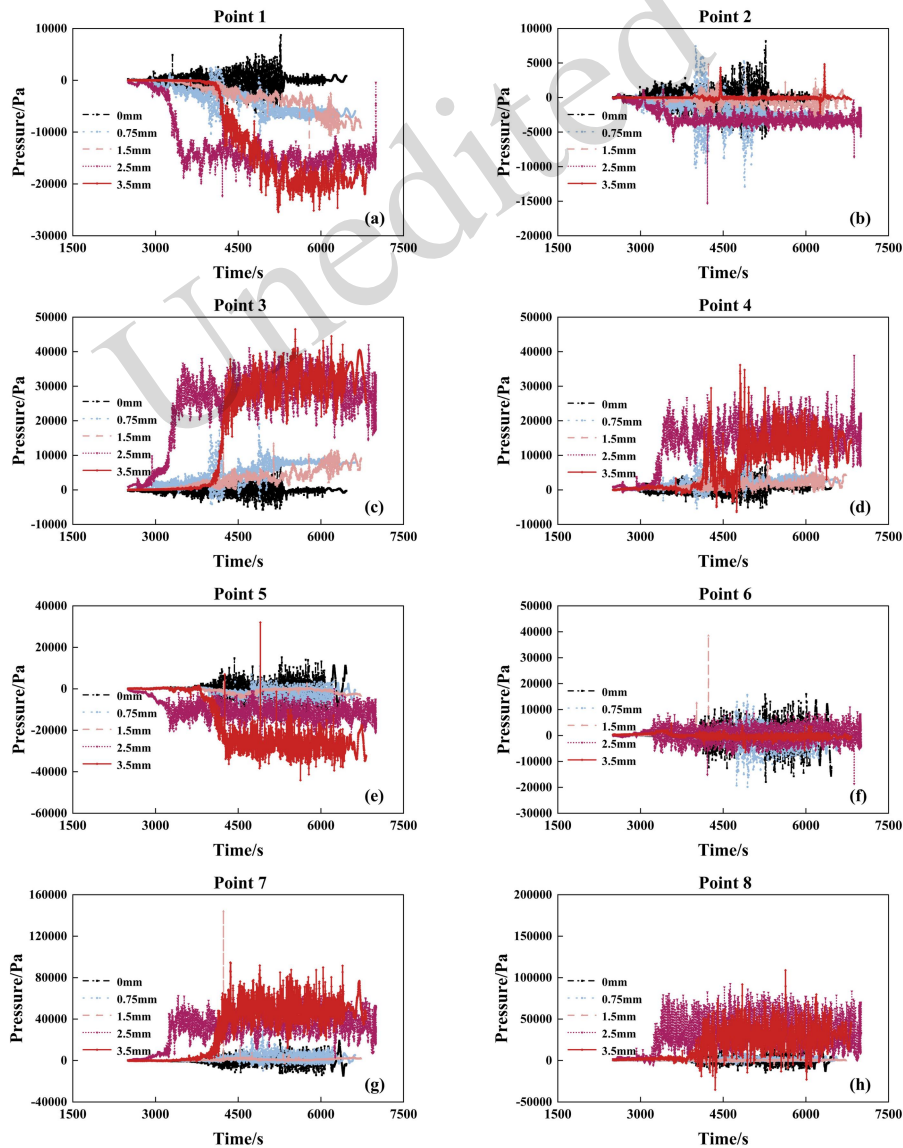


Fig. 7 EP2 pressure variation curves at the 8 monitoring points under different eccentricities (a) point 1 (b) point 2 (c)

point 3 (d) point 4 (e) point 5 (f) point 6 (g) point 7 (h) point 8
4.3.4 Impact of the number of injection points on sealing performance

Table 3 Boundary conditions with different numbers of injection ports

Number of injection ports	Injection ports per chamber	Single-pipe flow rate	Inner wall rotational speed
20	4	1.28mm/s	5r/min
40	8	0.64mm/s	5r/min
60	12	0.427mm/s	5r/min

The number of injection ports arranged around the periphery of the main drive sealing lubrication structure may affect the uniformity of grease distribution within the chamber. To investigate this, models were created with 4 and 12 evenly distributed injection ports per chamber. The inner cylinder was assigned a rotational boundary condition of 5 r/min, rotating positively around the X-axis for simulation. The results will later be compared with those from the original fluid domain model, in which 8 injection ports were distributed around each lubrication chamber in the same position as shown in Section 4.3.2, to analyze the influence of the number of injection ports on grease flow behavior.

For working conditions with different numbers of

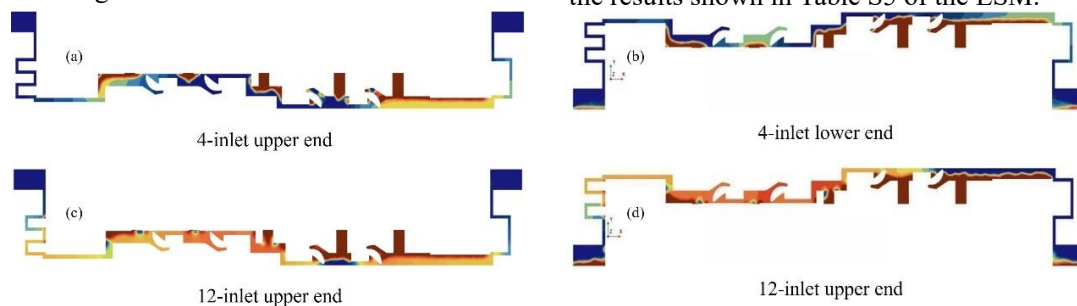


Fig. 8 EP2 grease distribution under different numbers of injection ports of fluid domain (a) 4-inlet upper end (b) 4-inlet lower end (c) 12-inlet upper end (d) 12-inlet lower end

The cavity filling rates of EP2 grease under three configurations with 4, 8, or 12 injection ports per chamber were compared (Table 4). With an increasing number of injection ports per chamber, the grease filling ratio at dynamic equilibrium in the main drive sealing system increased accordingly, leading to improved circumferential continuity. Therefore, the configuration with 12 injection ports per chamber is recommended for practical application.

injection ports (Table 3), the flow rate of grease through each port varied accordingly to ensure a consistent total grease flow within the chamber. In this study, we assumed that all injection ports had equal cross-sectional areas and that the inlet and outlet grease flow rates were identical.

Fig. 8 illustrates the grease distribution within the XOY cross-section of the chamber under two conditions: with 4 or 12 evenly distributed injection ports around a single chamber. When only 4 injection ports were arranged around each chamber, the limited number of peripheral inlets caused most of the injected grease to adhere to the outer wall near the injection points. During the steady outflow of grease from both outlets, only a small portion of the grease adhered to the inner wall, resulting in clearly visible unfilled cavity regions within the chamber. The amount of grease in such cases was insufficient to meet sealing requirements. In contrast, when more injection points were provided, the grease volume fraction on the sealed motor side increased significantly, and the grease distribution within each chamber became more uniform. Similarly, a series of cross-sections parallel to the YOZ plane were extracted from the volume fraction diagrams under both conditions for grease distribution analysis, with the results shown in Table S5 of the ESM.

Table 4 Cavity filled rate of EP2 grease

Injection ports per chamber	EP2 grease fill rate
4	48.71%
8	54.27%
12	60.79%

When four injection ports were arranged around each chamber, only a small lower portion of the flow

path between the inner and outer cylinders was filled with grease in each lubrication chamber, and most of the EP2 grease still failed to adhere to the inner wall. In contrast, with 12 injection ports arranged around

each chamber, the grease filling within each chamber improved significantly. However, due to the wider gap on the non-motor side, regions without grease adhesion to the inner wall persisted on that side.

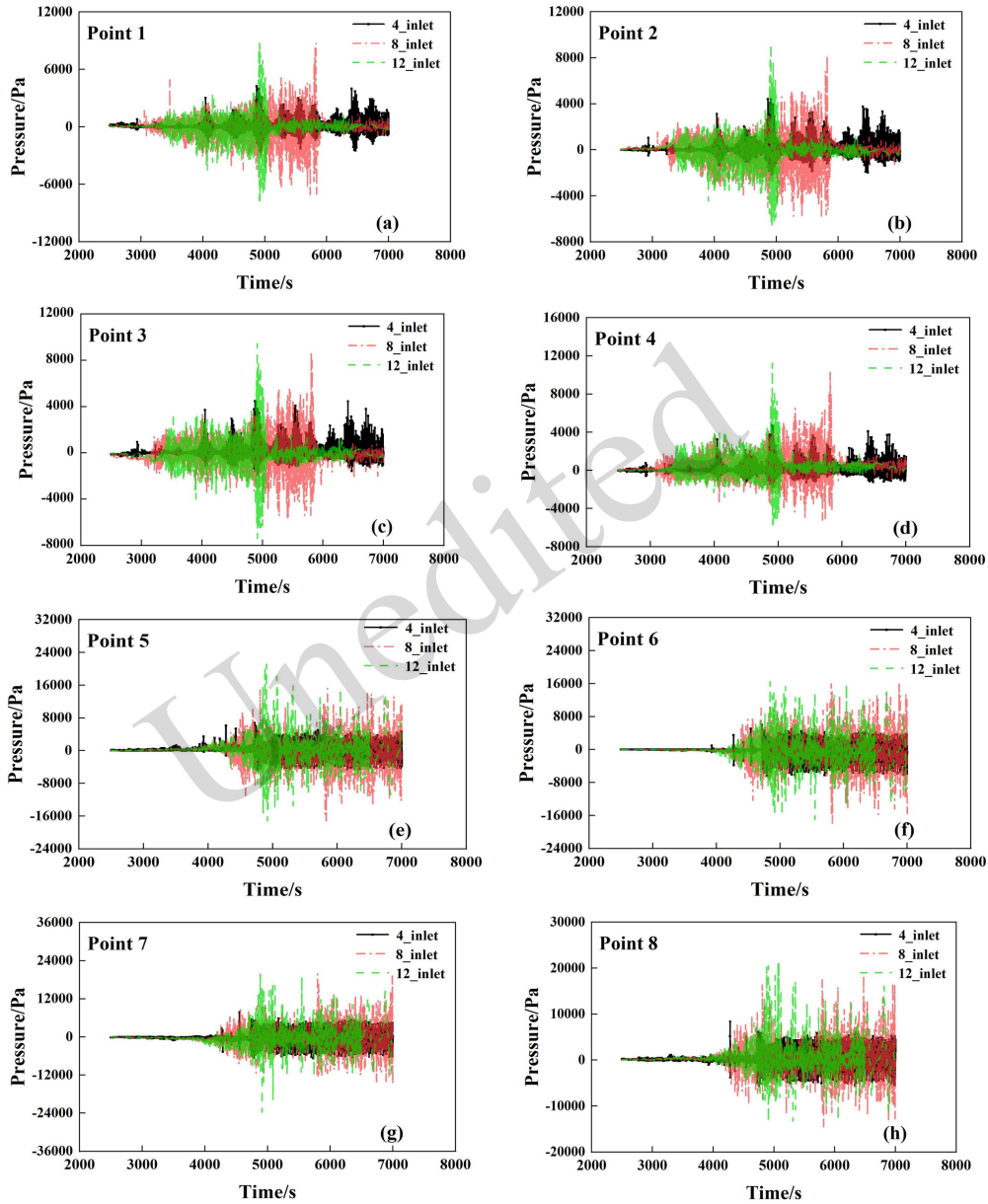


Fig. 9 Pressure variation at 8 monitoring points for three injection configurations (a) point 1 (b) point 2 (c) point 3 (d) point 4 (e) point 5 (f) point 6 (g) point 7 (h) point 8

The impact of the number of evenly distributed injection ports around the flow field on pressure variations at monitoring points on both sides of the fluid domain is shown in Fig. 9. Since the overall structure of the fluid domain remained largely unchanged, the pressure trends at each point were generally consistent across the three configurations.

As grease was injected, pressure fluctuations at the four monitoring points on the motor side gradually stabilized. In contrast, the structure on the non-motor side had a more pronounced influence on the pressure fluctuations at points 5, 6, 7, and 8. Notably, when 12 injection ports were evenly arranged around each chamber, the pressure variations on the non-motor

side became significantly more intense. Additionally, pressure values at the four non-motor side points began to fluctuate more noticeably around 3800 s, indicating a difference in grease filling efficiency between the two sides due to the structural differences in their flow paths. Grease began to diffuse and fill the motor side first.

4.3.5 Effect of inner wall rotational speed

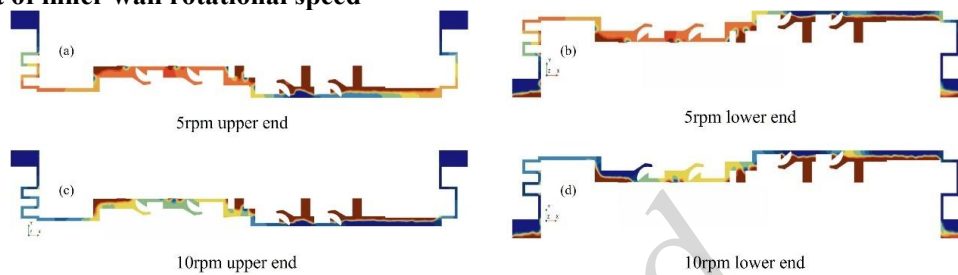


Fig. 10 EP2 grease distribution under different inner wall rotational speeds of fluid domain (a) 5r/min upper end (b) 5r/min lower end (c) 10r/min upper end (d) 10r/min lower end

Similarly, a series of cross-sections parallel to the YOZ plane were extracted from the volume fraction diagrams under both conditions for grease distribution analysis, with the results shown in Table S6 of the ESM. The effect of inner wall rotational speed on the pressure variation at monitoring points on both sides of the fluid domain is shown in Fig. 11. Comparing the pressure variations at each point, shows that with grease injection, increasing the motor-side rotational speed caused more pronounced pressure fluctuations at points 1, 2, 3, and 4, while the grease distribution on the non-motor side tended to become more uniform. Moreover, under the 10r/min condition, the mean pressure fluctuations were significantly higher than those at 5 r/min, indicating a deterioration in sealing performance. Therefore, reducing the rotational speed within a certain range can enhance the sealing characteristics of the main drive system.

5 Conclusions

In this study, we used the VOF multiphase flow model and finite element simulation software, Star CCM+, to analyze the simulation results of the grease injection process into the lubrication cavity of the main drive seal under different coaxial errors between the inner and outer cylinders. Additionally, we investigated the distribution of grease in the flow field

Fig. 10 illustrates the grease distribution within the XOY cross-section of the chamber under two conditions: with 5 or 10 revolutions per min. With increasing inner wall rotational speed, the annular distribution of grease was markedly reduced, and the grease tended to overflow more easily from the outlet, leading to a decrease in the volume fraction of EP2 grease.

and pressure characteristics under various numbers of injection ports and inner wall rotation speeds. The impact of these different operating conditions on the overall sealing and lubrication effectiveness of the structure was thoroughly examined, leading to the following conclusions:

1. When other conditions are constant, for the experimental workstation involved in this study, when there was a small range of variation in the eccentricity between the inner and outer sleeves (eccentricity variation not exceeding 0.75mm), the distribution of grease in the channels remained relatively uniform, ensuring a certain level of sealing. However, with a larger eccentricity, the grease distribution in the channel became uneven, and as the eccentricity increased, the positive and negative pressure zones formed by the grease in the cavity became more pronounced, making it difficult to maintain normal sealing lubrication. Therefore, efforts should be made to avoid significant variation in coaxial errors.

2. Under the condition of maintaining a constant total grease flow into the chamber, configurations with fewer injection ports arranged around each chamber resulted in poor grease distribution uniformity and limited diffusion toward both sides, making it difficult to meet actual sealing requirements. Increasing the number of peripheral injection ports effectively improved the uniformity of grease distribution within the chamber. However,

compared to modifying the original flow channel structure, increasing the number of injection ports offered only limited improvement in overall grease distribution. Since the number of injection ports significantly affected grease distribution, the pressure

values at monitoring points near both outlets also varied accordingly. In particular, the increase in the number of injection port had a more pronounced impact on pressure fluctuations at various locations on the non-motor sealing side.

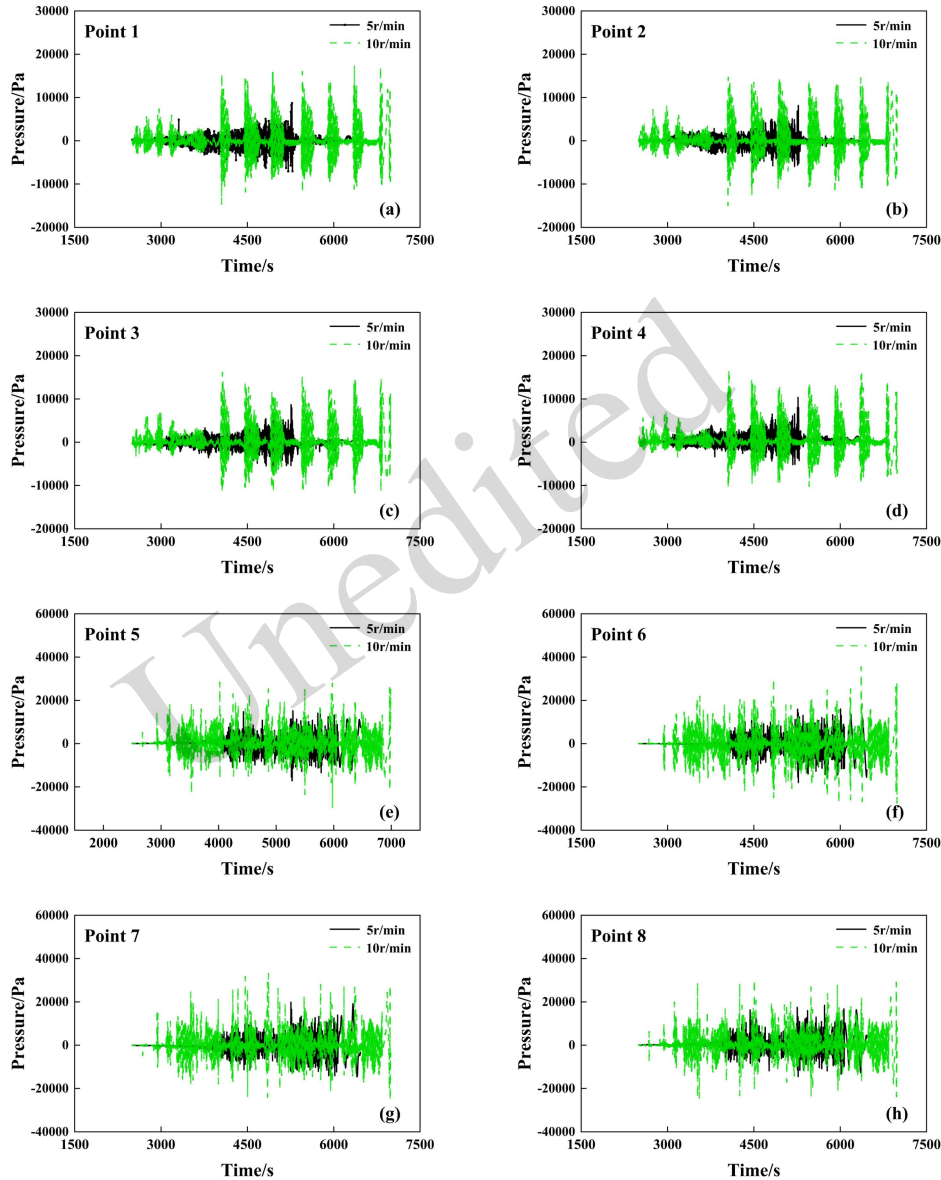


Fig. 11 Pressure variation at 8 monitoring points for two inner wall rotational speeds (a) point 1 (b) point 2 (c) point 3 (d) point 4 (e) point 5 (f) point 6 (g) point 7 (h) point 8

3. Changes in the inner wall rotational speed significantly affected grease distribution and sealing performance in the main drive system. Higher speeds reduced adhesion and annularity, leading to poorer sealing, with the motor side being more sensitive than the non-motor side. Hence, maintaining a lower rotational speed within a suitable range is advisable to

improve sealing reliability.

Acknowledgments

We acknowledge the support of the State Key R&D Project of Zhejiang Province (2024C01116, 2024C01120), and the Key R&D Project of Hangzhou (2023SZD0049, 2023SZD0111).

Author contributions

Zheming TONG and Yuchen ZHAO designed the research and wrote the first draft of the manuscript. Lianhui JIA and Xiaolei ZHOU coordinated responsibility for the project planning and execution. Haoxiang LU and Wenqi NIU processed the data and helped to organize the manuscript. Zheming TONG revised the final version and provided the funding support.

Conflict of interest

Zheming TONG, Yuchen ZHAO, Lianhui JIA, Xiaolei ZHOU, Haoxiang LU and Wenqi NIU declare that they have no conflict of interest.

References

- Agrawal AK, Murthy V.M.S.R, Chattopadhyaya S, et al., 2022. Prediction of TBM disc cutter wear and penetration rate in tunneling through hard and abrasive rock using multi-layer shallow neural network and response surface methods. *Rock Mechanics and Rock Engineering*, 55(6): 3489-3506.
- Ai YB, 2023. Cleanliness test and contaminant analysis of lubricant in main drive gearbox of shield. *Construction Machinery and Equipment*, 54(6): 104-108+112.
- Ariati R, Sales F, Souza A, et al., 2021. Polydimethylsiloxane composites characterization and its applications: A review. *Polymers*, 13(23): 1-21.
- Barzegari G, Khodayari J, Rostami J, 2021. Evaluation of TBM cutter wear in Naghadeh water conveyance tunnel and developing a new prediction model. *Rock Mechanics and Rock Engineering*, 54(12): 6281-6297.
- Borras FX, de Rooij MB, Schipper DJ, 2020. Misalignment induced micro-elastohydrodynamic lubrication in rotary lip seals. *Lubricants*, 8(2): 19.
- Dai Y, Tang RQ, Yu C, et al., 2025. Air-oil two-phase flow and oil penetration characteristics of angular contact ball bearing under oil jet lubrication: Numerical and experimental investigations. *Physics of Fluids*, 37(4). <https://doi.org/10.1063/5.0266444>
- Di Giorgio S, Pirozzoli S, Iafrati A, 2024. Evaluation of advection schemes and surface tension model for algebraic and geometric VOF multiphase flow solvers. *Journal of Computational Physics*, 499: 112717. <https://doi.org/10.1016/j.jcp.2023.112717>
- Gao WX, Deng LY, Zhang RL, 2008. Research on the seal structure of main bearing for TBM. *Mining & Processing Equipment*, 36(13): 21-23.
- Gong JF, Wang W, Wang F, et al., 2024. Statistics of China's railway tunnels by the end of 2023 and overview of tunnels of key new projects in 2023. *Tunnel Construction*, 44(2): 377.
- Guo FJ, Zhao YH, Zhang JJ, 2016. Comparative analysis of TBM main drive lubrication seal system. *Modern Manufacturing Technology and Equipment*, (1): 112-113+115. <https://doi.org/10.16107/j.cnki.mmte.2016.0051>
- Hand BP, Erdogan N, Murray D, et al., 2022. Experimental testing on the influence of shaft rotary lip seal misalignment for a marine hydro-kinetic turbine. *Sustainable Energy Technologies and Assessments*, 50: 101874.
- Ji JX, Su SD, Xiang C, et al., 2023. Study on fluid-solid-thermal coupling simulation of shield machine lip seal. *Lubrication Engineering*, 48(3): 48-54. <https://doi.org/0.3969/j.issn.0254-0150.2023.03.006>
- Jiang X, 2015. Shield main driving seal lubrication oil supply system improvement. *Construction Mechanization*, 36(12): 57-59.
- Li JB, 2021. Current status, problems and prospects of research, design, and manufacturing of boring machine in China. *Tunnel Construction*, 41(6): 877-896. <https://doi.org/10.3973/j.issn.2096-4498.2021.06.001>
- Li RJ, Shan RL, Li RS, et al., 2014. Key technology of shield machine main drive sealing. *Journal of Xi'an University of Science and Technology*, 34(5): 579-584. <https://doi.org/10.4028/www.scientific.net/AMM.580-583.1081>
- Li TM, Sun HB, Chen QK, et al., 2022. Comparative analysis of properties between two main bearing seals of large-diameter shield tunneling under high water pressure. *Tunnel Construction*, 42(S1): 517-525. <https://doi.org/10.3973/j.issn.2096-4498.2022.S1.061>
- Li YH, Wang TM, Chen SB, et al., 2024. Dry friction thermal behavior and wear mechanism of polyurethane elastomer for main drive seal of TBM. *Tribology International*, 193: 109367. <https://doi.org/10.1016/j.triboint.2024.109367>
- Liu WX, Hu HX, Zhuang YS, et al., 2013. Main drive seal system analysis of tunnel machine. *Machinery*, 40(6): 76-80.
- Liu XR, Yu PD, Zhang LF, et al., 2022. Research on main drive pressure compensation system of high pressure slurry balance shield machine. *Chinese Hydraulics & Pneumatics*, 46(11): 175-180.
- Liu XY, Li L, Sun HB, et al., 2022. Typical failure case analysis of shield main bearing. *Construction Mechanization*, 43(3): 73-75.
- Ma H, 2018. Thoughts on key technologies for sealing maintenance and renovation of shield machine main drive. *China Plant Engineering*, (6): 63-64. <https://doi.org/10.35696/1915-000-007-014>
- Naheed S, Zuber M, Barikani M, et al., 2021. Molecular engineering and morphology of polyurethane elastomers containing various molecular weight of macrodiol. *Materials Science and Engineering: B*, 264: 114960.
- Nilot AE, Li EY, Fang G, et al., 2024. Inverting continuous in-tunnel passive seismic data for velocity structure mapping ahead of the TBM cutterhead. *Tunnelling and Underground Space Technology*, 151: 105855.
- Pinedo B, Conte M, Aguirrebeitia J, et al., 2017. Effect of misalignments on the tribological performance of elastomeric rod lip seals: study methodology and case

- study. *Tribology International*, 116: 9-18.
- Song YC, Wang CH, Ning Z, 2011. Combined level set-VOF method used in the computation of incompressible two-phase flows. *Journal of Combustion Science and Technology*, 17(5): 443-450.
- Stakenborg MJL, Van Leeuwen HJ, ten Hagen EAM, 1990. Visco-elastohydrodynamic (VEHD) lubrication in radial lip seals: Part 1-Steady-state dynamic viscoelastic seal behavior. *Journal of Tribology*, 112(4): 578-583.
- Tan F, Yang B, Huang L, et al., 2022. Study on the structure optimization of shield tunneling machine's main drive seal. *Lubrication Engineering*, 47(4): 116-123.
- Tang PX, Li ZMQ, Hou, XY, et al., 2024. Influence of Oil Injection Lubrication Parameters of High-Speed Internal Meshing Gear Based on the Computational Fluid Dynamics. *Lubricants*, 12(11): 390.
- Tasora A, Prati E, Marin T, 2013. A method for the characterization of static elastomeric lip seal deformation. *Tribology International*, 60: 119-126.
- Tong SG, Fu ZL, Tong ZM, et al., 2023. Fault diagnosis for gearboxes based on Fourier decomposition method and resonance demodulation. *Journal of Zhejiang University: Science A*, 24(5):404-418.
- Van Leeuwen HJ, Stakenborg MJL, 1990. Visco elastohydrodynamic (VEHD) lubrication in radial lip seals: part 2-fluid film formation. *Journal of Tribology*, 112(4): 584-592.
- Vishwakarma M, Purohit R, Harshlata V, et al., 2017. Vibration analysis & condition monitoring for rotating machines: a review. *Materials Today: Proceedings*, 4(2): 2659-2664.
- Wang CL, 2021. Key technology of EPB's drive unit sealing optimization in deep buried area. *Construction Mechanization*, 42(5): 41-44.
- Wang DZ, Li WL, Qiu ZW, et al., 2023. Fluid-structure coupling simulation of the main drive seal in shield machine. 2023 3rd International Conference on Robotics, Automation and Artificial Intelligence, RAAI: 87-90.
- Wang JH, 2021. Research on optimization and modification technology of internal sealing labyrinth structure of TBM main bearing. *Railway Construction Technology*, (2): 77-79+123.
- Wang JS, Zhong YC, 2021. VOF application for capturing interface in two-phase flow. *Machine Building & Automation*, 50(6): 129-134.
- Wang XM, Wang ZS, Wang Q, et al., 2020. Prediction of oil consumption in the cross river section of slurry shield tunneling machine based on IAFSA-BP neural network. *Highway*, 65(11): 379-385.
- Wu B, Zhang N, 2022. Study on PUE sealing material for the main drive of roadheader. *Polyurethane Industry*, 37(1): 16-19.
- Xiang C, Long WY, Guo F, et al., 2023. Fluid-structure interaction simulation of sealing shield main drive seal properties. *JTsinghuaUniv(Sci&Technol)*, 63(1): 71-77.
- Xu FC, 2021. Experimental study on main drive seal lubrication system of tunneling Machine. *Tunnel Construction*, 41: 70-74.
- Yao P, 2021. Response measures and research on main drive seal failure of shield machine in water-rich strata. *Construction Mechanization*, 42(7): 20-23.
- Yuan XL, 2020. Comparison and analysis of the main driving sealing form of shield machine. *Construction Mechanization*, 41(4): 20-21.
- Zeng YJ, 2021. Study on wear-resisting belt technology of shield machine main drive support ring. *Railway Construction Technology*, (5): 28-30+54.
- Zhang HG, 2018. Leakage fault treatment for the main bearing sealing system of a shield machine. *Modern Tunnelling Technology*, 55(4): 216-220.
- Zhang MM, Sun J, Chen WY, 2019. An interface tracking method of coupled youngs-VOF and level set based on geometric reconstruction. *Chinese Journal of Theoretical and Applied Mechanics*, 51(3): 775-786.
- Zhang QL, Zhu HX, 2023. Research and optimization of sealing performance of VD ring for main drive of shield machine. *Lubrication Engineering*, 48(3): 157-163.
- Zhang XL, Shap YL, Xu SJ, 2022. Innovative design of seal-installation-device in main drive based on TRIZ. *Modern Manufacturing Technology and Equipment*, 58(8): 69-72.
- Zhang YK, Gong GF, Yang HY, et al., 2024. From tunnel boring machine to tunnel boring robot: perspectives on intelligent shield machine and its smart operation. *Journal of Zhejiang University: Science A*, 25(5): 357-381.
- Zhang ZH, Zheng J, Ren Y, et al., 2021. Optimization of main drive seals in shields. *Tunnel Construction*, 41(6): 1065-1070.
<https://doi.org/10.3973/j.issn.2096-4498.2021.06.020>
- Zhao YC, Tong ZM, Tong SG, et al., 2026. Research on hard-rock breaking status under different position relationships of TBM disc cutter and rock's normal plane in various groove spacings by abrasive water jet. *Tunnelling and Underground Space Technology*, 167:107052. <https://doi.org/10.1016/j.tust.2025.107052>
- Zhou XH, Zhang YK, Gong GF, et al., 2025. Impact of disc-cutter partial wear on tunneling parameters and a high-accuracy method for discrimination of partial wear. *Journal of Zhejiang University: Science A*, 26(4): 359-375.
- Zhu L, Huang TZ, Liang L, 2017. A hybrid-mesh hybridizable discontinuous Galerkin method for solving the time-harmonic Maxwell's equations. *Applied Mathematics Letters*, 68: 109-116.
- Zhu WL, Zhu RP, Tang X, et al., 2022. CFD-based analysis of oil and gas two-phase flow characteristics in double-row tapered roller bearings with different rib structures. *Applied Sciences*, 12(3): 1156.

Electronic supplementary materials

Sections S1-S5, Tables S1-S6, Figures S1-S7

中文概要

题目: 隧道掘进机主传动密封润滑结构注脂过程的仿真与实验分析

作者: 童哲铭^{1,2}, 赵宇琛^{1,2}, 贾连辉³, 周小磊³, 卢浩翔^{1,2}, 牛文琪³

机构: ¹浙江大学, 流体动力与机电系统国家重点实验室, 中国杭州, 310027; ²浙江大学, 机械工程学院, 中国杭州, 310027; ³中铁工程装备集团有限公司, 中国郑州, 450016

目的: 在隧道掘进机(TBM)的开挖过程中, 构成主传动密封润滑结构的装配部件的制造精度和精度, 以及操作条件, 直接影响整体密封性能。这反过来又会影响主轴承和整个TBM的寿命。模拟在不同工作条件下将润滑脂注入主传动密封润滑室内部结构的过程至关重要。分析腔室内润滑脂的分布和系统内的压力分布可以提高主驱动密封结构防止外部污染物渗透的能力, 最终延长主驱动结构的寿命。

创新点: 1. 本研究将VOF多相流模拟和实验研究相结合, 系统分析了不同偏心率、注脂口数量和内壁转速对EP2润滑脂分布的影响; 2. 建立试验模型, 成功模拟EP2油脂注入主驱动腔体工艺过程。

方法: 1. 使用VOF多相流模型和有限元模拟软件StarCCM+分析了在内筒和外筒之间不同同轴误差下向主传动密封润滑腔注入润滑脂过程的模拟结果; 2. 研究了不同注入口数量和内壁转速下润滑脂在流场中的分布和压力特性 3. 彻底检查了这些不同操作条件对结构整体密封和润滑效果的影响。

结论: 1. 当内外套筒之间的偏心距变化范围很小(不超过0.75mm)时, 润滑脂在通道中的分布保持相对均匀, 确保了一定程度的密封。然而, 随着偏心率的增加, 通道中的润滑脂分布变得不均匀, 随着偏心度的增加, 腔内润滑脂形成的正负压区变得更加明显, 难以保持正常的密封润滑, 应努力避免同轴误差的显著变化。2. 在保持进入腔室的总润滑脂流量恒定的情况下, 每个腔室周围布置的注入口较少的配置导致润滑脂分布均匀性差, 向两侧的扩散有限, 难以满足实际的密封要求。增加外围注入口的数量有效地提高了腔室内润滑脂分布的均匀性。然而, 与修改原始流道结构相比, 增加注入口的数量对整体润滑脂分布的改善有限。由于注入口的数量显著

影响了润滑脂的分布, 因此两个出口附近的监测点的压力值也随之变化。特别是, 喷射口数量的增加对非电机密封侧各个位置的压力波动产生了更明显的影响。3. 内壁转速的变化显著影响了主传动系统中的润滑脂分布和密封性能。较高的速度会降低附着力和环刚度, 导致密封性较差, 电机侧比非电机侧更敏感。因此, 建议将较低的转速保持在适当的范围内, 以提高密封可靠性。

关键词: 隧道掘进机(TBM); 主驱动密封润滑结构; EP2油脂加注; 润滑脂优化实验分析